The Origin of Outflows in Evolved Stars
Proceedings IAU Symposium No. 366, 2022
L. Decin, A. Zijlstra & C. Gielen, eds.
doi:10.1017/S1743921322000783

Effects of wind mass-loss on the observational properties of Type Ib and Ic supernova progenitors

Sung-Chul Yoon[1], Moo-Keon Jung[1], Harim Jin[1,2] and Hyun-Jeong Kim[3]

[1]Department of Physics and Astronomy, Seoul National University, 08826, Seoul, South Korea
email: scyoon@snu.ac.kr

[2]Argelander Institute for Astronomy, University of Bonn, D-53121, Bonn, Germany

[3]Korea Astronomy and Space Science Institute, 34055, Daejeon, South Korea

Abstract. Progenitors of Type Ib and Ic supernovae (SNe) are stripped envelope stars and provide important clues on the mass-loss history of massive stars. Direct observations of the progenitors before the supernova explosion would provide strong constraints on the exact nature of SN Ib/Ic progenitors. Given that stripped envelope massive stars can have an optically thick wind as in the case of Wolf-Rayet stars, the influence of the wind on the observational properties needs to be properly considered to correctly infer progenitor properties from pre-SN observations. Non-LTE stellar atmosphere models indicate that the optical brightness could be greatly enhanced with an optically thick wind because of lifting-up of the photosphere from the stellar surface to the wind matter, and line and free-free emissions. So far, only a limited number of SN Ib/Ic progenitor candidates have been reported, including iPTF13bvn, SN 2017ein and SN 2019yvr. We argue that these three candidates are a biased sample, being unusually bright in the optical compared to what is expected from typical SN Ib/Ic progenitors, and that mass-loss enhancement during the final evolutionary stage can explain their optical properties.

Keywords. Massive Stars, Wolf-Rayet stars, Hydrogen deficient stars, Stellar atmosphere, Stellar evolution, Stellar mass loss, Type Ib supernovae, Type Ic supernovae

1. Introduction

The evolution of massive stars is affected by their mass-loss history. Mass loss from massive stars can be caused by various factors like radiation-driven stellar winds, stellar pulsation, rapid rotation, episodic mass eruptions, and binary interactions (e.g., Langer 2012; Smith 2014; Vink 2022). The resulting different final structures of massive stars largely determine the observational diversity of core-collapse supernovae (ccSNe). For example, Type IIP and IIb supernovae would result from progenitors having large (i.e., several solar masses) and small (less than one solar mass) amounts of hydrogen in their envelopes, respectively. Type Ib and Ic supernovae (SNe Ib/Ic) are characterized by absence of hydrogen lines in the SN spectra, implying that their progenitors are helium stars whose hydrogen envelopes were stripped off before the SN explosion.

Direct identifications of ccSN progenitors are crucial for constraining theoretical predictions of massive star evolution, as it would reveal what SN progenitors look like immediately before the SN explosion for different SN types. Many SN II progenitors have been detected in pre-SN images (see Smartt 2015 for a review). By contrast, searches for

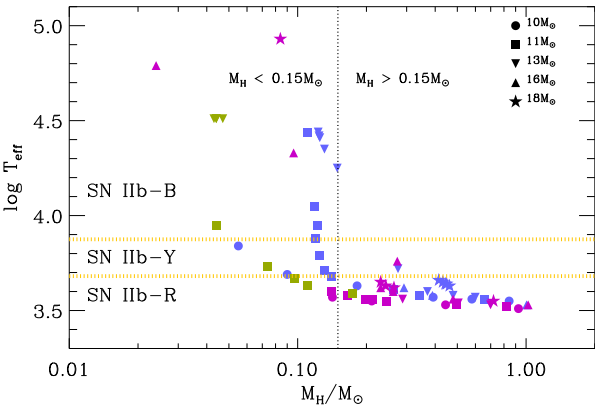

Figure 1. Surface temperatures of massive stars at the pre-SN stage as a function of the remaining hydrogen envelope mass, predicted by binary evolution models where mass loss due to Case B mass transfer from the primary star is considered. The models presented in this figure represent SN IIb progenitors whose hydrogen envelope mass is less than $1.0 M_{\odot}$. Different symbols indicate the initial masses of the primary stars of the binary models as indicated by the labels. Purple and Blue denote solar and LMC metalicity models, respectively. Green denotes solar metallicity models with a WR mass loss-rate reduced by a factor of 2 compared to the standard one. The orange dotted lines mark the boundaries for yellow supergiants: $3.681 \leq \log T_{\rm eff}/{\rm K} \leq 3.875$. The back dotted vertical line roughly defines the boundary between red supergiant progenitors and more compact (i.e., yellow/blue supergiant) progenitors. The figure is taken from Yoon *et al.* (2017).

SN Ib/Ic progenitors have been futile (Eldridge *et al.* 2013), except for a few cases including those of iPTF13bvn (Cao *et al.* 2013; Eldridge & Maund 2016; Folatelli *et al.* 2016), SN 2017ein (Kilpatrick *et al.* 2018; Van Dyk *et al.* 2018), and SN 2019yvr (Kilpatrick *et al.* 2021). This is often interpreted as evidence for relatively low-mass helium star progenitors produced in binary systems (e.g., Eldridge *et al.* 2013) rather than Wolf-Rayet (WR) star-like progenitors ($M \gtrsim 8\ M_{\odot}$). Studies of SNe Ib/Ic also imply relatively low SN ejecta masses for most cases (i.e., $M_{\rm ej} \approx 1.0 \cdots 4.0 M_{\odot}$) in favor of the binary scenario (e.g., Drout *et al.* 2011; Cano 2013; Lyman *et al.* 2016; Taddia *et al.* 2018; Prentice *et al.* 2019).

However, it should be noted that helium stars are not necessarily brighter in the optical for a higher mass, as pointed out by Yoon *et al.* (2012). This is because helium star spectra depend on the structure of the outermost layers and the presence of optically thick winds as discussed below. A careful study on the details of SN Ib/Ic progenitors is therefore needed for properly guiding future searches of SN Ib/Ic progenitors.

2. SN Ib/Ic progenitor properties

Many SN II progenitors, having an extended hydrogen envelope with a radius of $R >\sim 100\ R_{\odot}$, are found to be yellow or red supergiants (e.g., Smartt 2015). Stellar evolution models also predict that most massive stars at the pre-SN stage would be observed as red or yellow supergiants as long as the retained hydrogen envelope mass is higher than about $0.05 \cdots 0.10 M_{\odot}$ (Figure 1; e.g., Yoon *et al.* 2017; Farrell *et al.* 2020), with the exception of blue supergiant progenitors of 1987A-like peculiar SNe IIP which presumably originate from binary mergers (e.g., Podsiadlowski *et al.* 1990; Morris & Podsiadlowski 2007; Menon & Heger 2017; Urushibata *et al.* 2018).

By contrast, hydrogen-deficient SN Ib/Ic progenitors are relatively compact ($R <\sim 10\ R_{\odot}$; e.g., Yoon *et al.* 2010). Their surfaces are therefore hotter ($T_{\rm eff} >\sim 10^4$ K) than most SN II progenitors ($T_{\rm eff} < 10^4$ K). The resulting spectra from SN Ib/Ic progenitors

https://doi.org/10.1017/S1743921322000783 Published online by Cambridge University Press

would be much harder, leading to fainter optical brightness compared to the case of SN II progenitors for a given bolometric luminosity (e.g., Yoon *et al.* 2012). It is not surprising, therefore, that SN Ib/Ic progenitors have proven more difficult to identify than SN II progenitors in optical images.

The surface properties of SN Ib/Ic progenitors depend on their final mass and chemical composition. In Figure 2, the final luminosity and radius of helium-rich (i.e., $M_{\rm He} \gtrsim 1.0\ M_{\odot}$) SN Ib progenitors predicted by stellar evolution models of Yoon *et al.* (2017) are presented. The bolometric luminosity is proportional to the mass, which is a common feature of all stars in hydrostatic and thermal equilibrium. However, the radius decreases with increasing mass. This is a result of the so-called mirror effect: the carbon-oxygen core becomes more compact for a lower mass while the helium envelope becomes more extended. This has an important consequence for the optical brightness: SN Ib progenitors would be systematically brighter in the optical for a lower final mass as shown in the figure. In other words, relatively low-mass SN Ib progenitors might be easier to detect in pre-SN images despite the fact that more massive progenitors would have higher bolometric luminosities, unless the effects of optically thick winds are significant as discussed below.

On the other hand, SN Ic progenitors would be more compact and hotter than SN Ib progenitors if they were helium-poor carbon-oxygen stars as often assumed in the literature. This could make them even fainter in the optical than SN Ib progenitors as discussed in Yoon *et al.* (2012). In sharp contrast to SN Ib progenitors having a helium-rich envelope which is larger for a lower mass, the radius of helium deficient carbon-oxygen (CO) stars becomes smaller for a lower mass (see Jung *et al.* 2022). Therefore, among SN Ic progenitors, a lower mass progenitor would be fainter.

There also exists the possibility that a large amount of helium is retained in SN Ic progenitors, which can be hidden in the optical spectra. The photosphere temperature of SNe Ib/Ic near the optical peak is not high enough (i.e., $T_{\rm phot} \sim 7000 - 8000$ K) to make He I absorption lines by thermal processes. Non-thermal processes induced by radioactive ^{56}Ni are therefore invoked to explain He I lines of SNe Ib (Lucy 1991; Swartz 1991). This requires mixing of ^{56}Ni into the helium-rich layer in the SN ejecta, and otherwise He I lines would not be formed (Dessart *et al.* 2012; Hachinger *et al.* 2012; Teffs *et al.* 2020; Williamson *et al.* 2021).

Several studies, however, provide evidence that SN Ic progenitors are distinct from SN Ib progenitors in terms of helium-richness (e.g., Liu *et al.* 2016; Fremling *et al.* 2018; Yoon *et al.* 2019; Dessart *et al.* 2020; Shahbandeh *et al.* 2021). For example, Shahbandeh *et al.* (2021) find dichotomy in the strength of He I λ2.0581 μm line in near infrared (NIR) early-time spectra between SN Ib and SN Ic: this line is systematically weaker in SNe Ic than in SNe Ib. This can be considered strong evidence for the helium-poor nature of SN Ic progenitors because unlike the case of the He I lines in the optical, helium would be relatively easy to detect with the He I λ2.0581 μm line (e.g., Dessart *et al.* 2020).

The systematic difference between SNe Ic and Ib is also found in their photometric colors as shown in Figure 3. It is observed that the $B-V$ color of SNe Ic is systematically redder compared to SNe Ib (i.e., $\Delta(B-V) \approx 0.15$) at the V-band peak. A study on radiation-hydrodynamics simulations of SNe Ib/Ic by Jin & Yoon (2022, in preparation) concludes that this color difference can be best explained by helium-rich and helium-poor progenitors for SNe Ib and Ic, respectively. In this case, the photosphere of a SN Ib during the photospheric phase would be located at a relatively deeper and hotter layer than that of a corresponding SN Ic, making SNe Ib systematically bluer than SNe Ic at the optical peak. This is because the outer layer of the SN Ib ejecta where the photosphere is formed is more transparent than SNe Ic.

https://doi.org/10.1017/S1743921322000783 Published online by Cambridge University Press

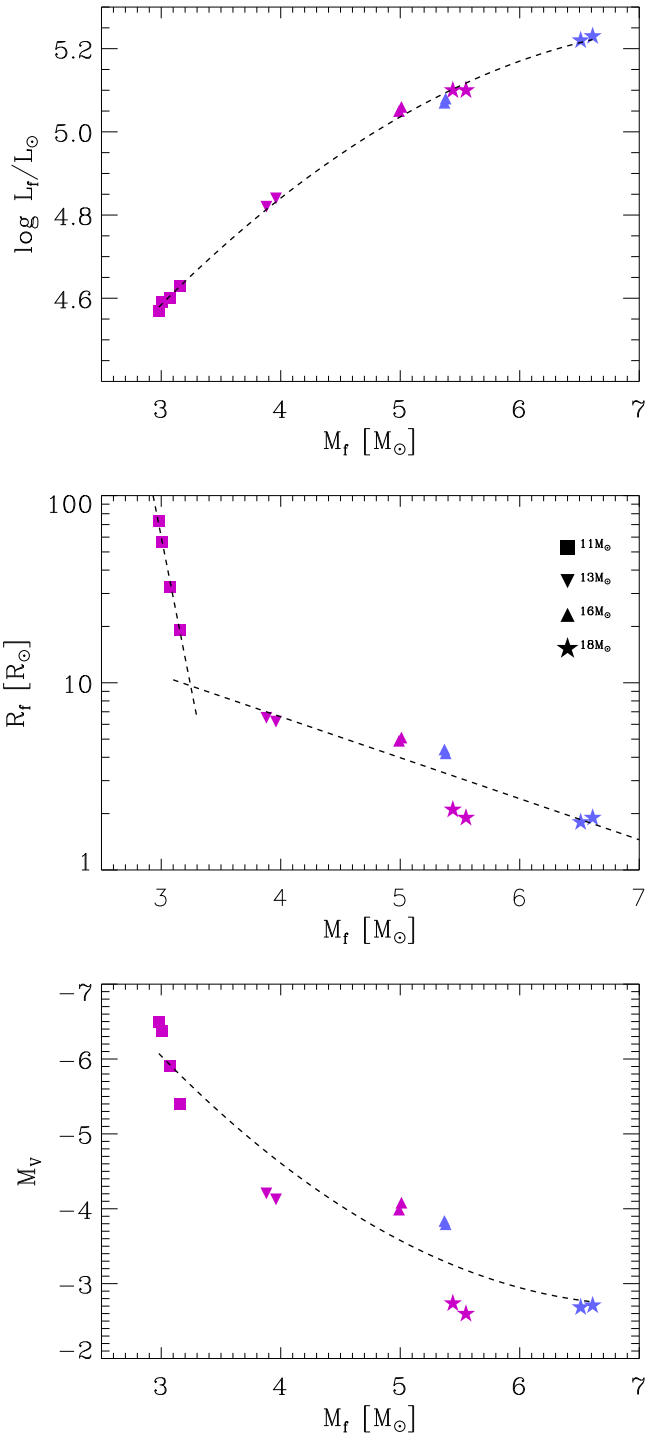

Figure 2. *Top panel:* Final luminosity as a function of the final mass of helium-rich (i.e., $M_{\rm He} \gtrsim 1.0 M_\odot$) SN Ib progenitors at the pre-SN stage predicted by binary stellar evolution models. *Middle panel:* The predicted final radius v.s. final mass relation of the corresponding models. *Bottom panel:* The corresponding V-band magnitude as a function of the final mass under the black-body approximation. The figure is taken from Yoon *et al.* (2017).

https://doi.org/10.1017/S1743921322000783 Published online by Cambridge University Press

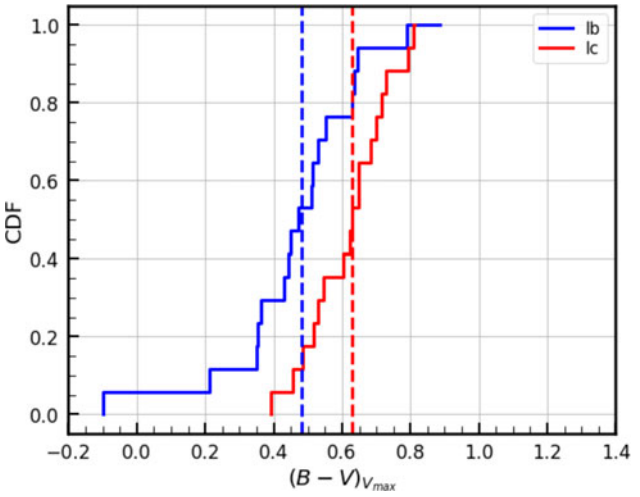

Figure 3. Cumulative distributions of the $B-V$ magnitude difference of SNe Ib and Ic at the peak of V-band magnitude. The SN sample is collected from the literature. See Jin & Yoon (2022, in preparation) for details.

The dichotomy of helium contents in SN Ib/Ic progenitors can also be inferred from the SN color evolution. Yoon *et al.* (2019) show that the color evolution of SNe Ib/Ic during early times is significantly affected by a ^{56}Ni mixing. If ^{56}Ni remains deep inside the SN ejecta, the photosheric color of a SN Ib/Ic would become quickly red initially because of the cooling induced by the ejecta expansion. But it becomes blue several days later when the photosphere recedes to the inner layer heated by ^{56}Ni. By contrast, if ^{56}Ni is fully mixed into the outermost layers of the ejecta, the color evolution becomes monotonic from blue to red color during the photospheric phase. Comparison with observations implies a strong ^{56}Ni mixing in several SNe Ic where monotonic color evolution is found, in which case optical He I lines would be easily produced even with a relatively small amount of helium (Figure 4). This indicates that SNe Ic progenitors are indeed helium-poor.

3. Evolution of massive stars towards SNe Ib/Ic

SN Ib/Ic progenitors lose their hydrogen envelopes during the post-main sequence phase. For single stars at solar metallicity, this can be realized by stellar winds if the initial mass is higher than about $25 \cdots 40\ M_{\odot}$, depending on the uncertain mass-loss rate from supergiant stars (see Yoon 2015 for a review). In close binary systems, mass transfer during the post-main sequence phase (mostly during helium core contraction and core helium burning phase: so-called Case B mass transfer) can remove a large fraction of the hydrogen envelope. The amount of the remaining hydrogen in the envelope after the mass transfer phase depends on the initial parameters of the binary system including the primary mass, mass ratio, and initial period (e.g., Yoon *et al.* 2017). The stripped star would eventually become a pure helium star if all hydrogen is removed from the surface via winds and/or further mass transfer during the post core helium burning phase. Figure 5 provides an example on how the predicted final fates of primary stars in close binary systems depend on the initial mass and orbital period. However, it should be noted that the parameter space for producing pure helium stars would depend on the uncertain mass-loss rate at the post-mass transfer stage (e.g., Vink 2017; Gilkis *et al.* 2019).

The evolution thereafter is largely determined by the mass loss history from helium stars. The dependence of the mass-loss rate of helium stars on the physical conditions

https://doi.org/10.1017/S1743921322000783 Published online by Cambridge University Press

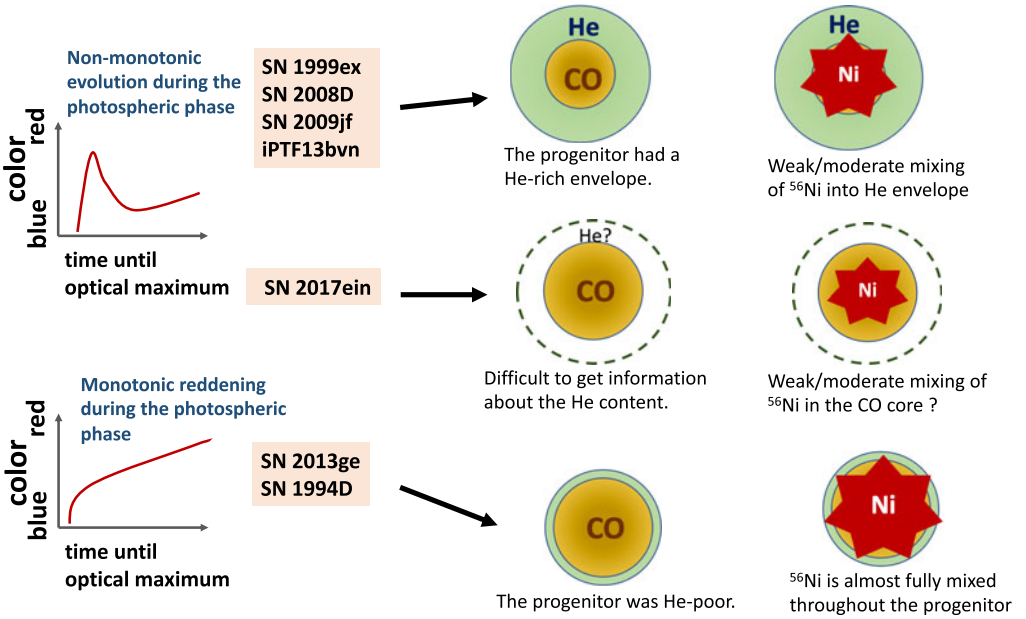

Figure 4. Schematic illustration of the color evolution of SNe Ib and Ic according to the degree of ^{56}Ni mixing in the ejecta (the figures in the left side) according to the numerical result of Yoon *et al.* (2019). Comparison with the observed color evolution implies a relatively weak/moderate ^{56}Ni mixing for SNe Ib and a very strong mixing for some SNe Ic (SN 2013ge and SN 1994D). Given that non-thermal processes due to radioactive ^{56}Ni play an essential role for the formation of He I lines, this result indicates that these SNe Ic had helium-poor progenitors, while SNe Ib had helium-rich progenitors. The figure is taken from Yoon *et al.* (2019).

and different evolutionary stages is not fully understood yet while great progress is being made in this direction (see Vink 2022 for a recent review). Stellar evolution models still cannot provide a robust prediction on whether or not SN Ib and Ic progenitors form a continuous sequence in terms of helium contents.

If the helium star mass is higher than a certain limit (e.g., about $8M_{\odot}$ for solar metallicity; see Shenar *et al.* 2020; Aguilera-Dena *et al.* 2021 for recent related discussions), the mass-loss rate would be high enough for the helium star to appear as a WR star that is characterized by strong emission lines from an optically thick wind. The WR mass-loss rate has been inferred by many observational studies on WR stars in the local Universe. Recently, Yoon (2017) argued, based on the observed WR star sample given by the Potsdam group (Hamann *et al.* 2006; Sander *et al.* 2012; Hainich *et al.* 2014), that the WR mass-loss rate would be enhanced when WR stars undergo a transition from the WN to WC phase (see, however, Sander *et al.* 2020). As shown in Figure 6, a clear dichotomy in the amount of helium is found in the evolutionary models of helium stars using the WR mass-loss rate prescription that includes the effect of the mass-loss enhancement in the WC phase (see also Woosley 2019). This result is consistent with the conclusions of the above-mentioned SN studies on the helium dichotomy between SNe Ib and Ic.

4. Effects of winds on the optical properties of SN Ib/Ic progenitors

As discussed above, SN Ib/Ic progenitors are relatively compact ($R <\sim 10R_{\odot}$) compared to SN II progenitors. Among SN Ib and Ic progenitors, SN Ic progenitors would

https://doi.org/10.1017/S1743921322000783 Published online by Cambridge University Press

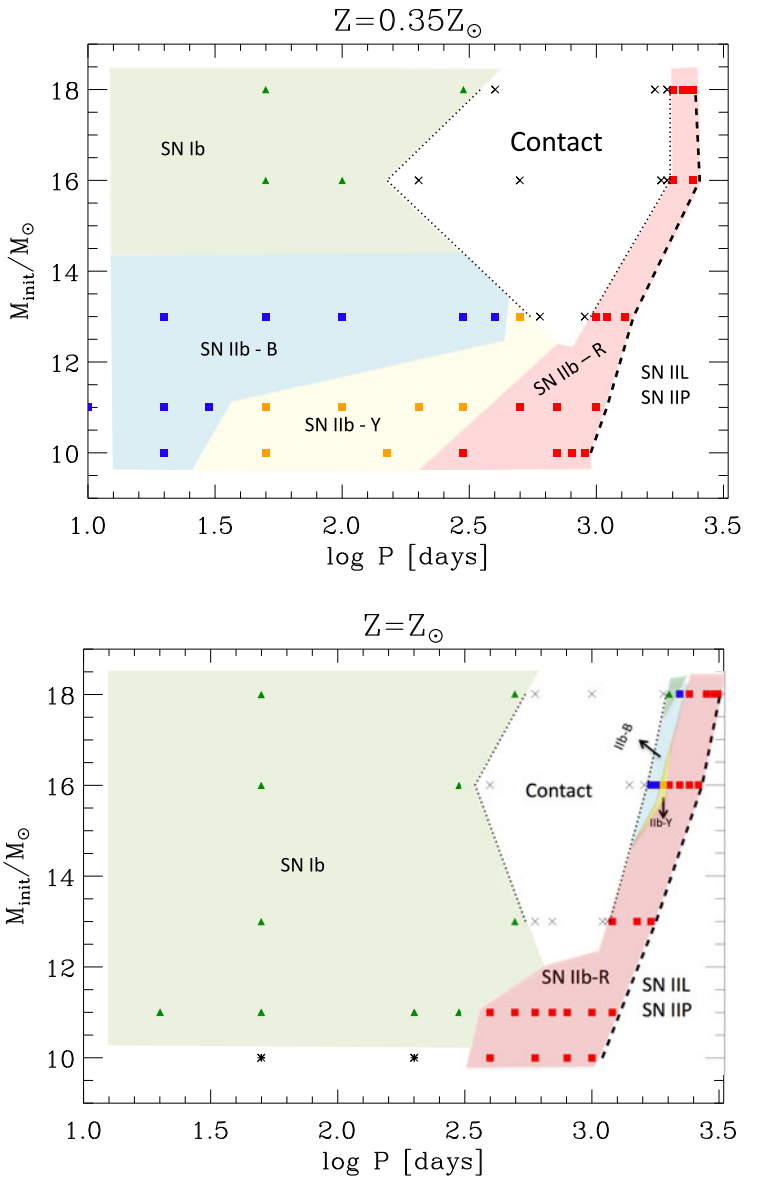

Figure 5. Final fates of primary stars in close binary systems predicted by stellar evolution models for two different metallicities (LMC and solar metallicities for the upper and lower panels, respectively), in the plane spanned by the initial primary star mass and the initial orbital period. In the models, a fixed mass ratio of $q = 0.9$ (the ratio of the secondary to the primary star masses) and mass accretion efficiency of $\beta = 0.2$ (i.e., the ratio of the accreted to the transferred masses) are assumed. Different fates are indicated by different colors as indicated by the labels. SN IIb-B, IIb-Y and II-R denotes SN IIb from blue, yellow and red supergiant progenitors, resepctively. The figure is taken from Yoon *et al.* (2017).

be more compact ($R < 1.0 R_\odot$) than SN Ib progenitors. Under the black body approximation, therefore, the optical brightness would decrease in the order of SN II, Ib and Ic progenitors for a given bolometric luminosity.

However, massive helium stars like WR stars may have an optically thick wind if the luminosity is sufficiently high. Such a wind can significantly affect the optical brightness and color, because of the following reasons (Kim *et al.* 2015; Jung *et al.* 2022):

https://doi.org/10.1017/S1743921322000783 Published online by Cambridge University Press

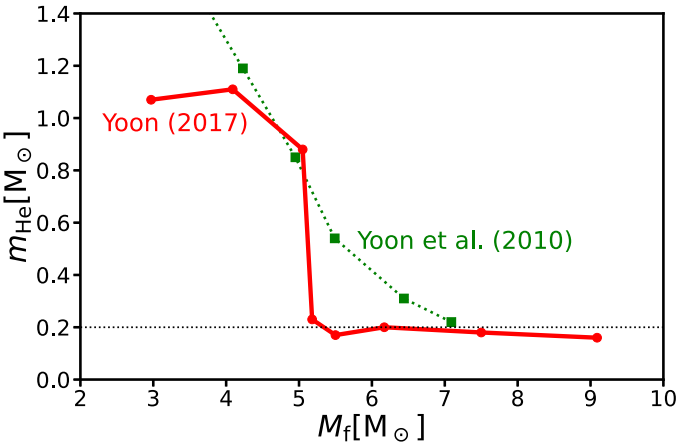

Figure 6. Amounts of helium retained in helium star models at the pre-SN stage as a function of the final mass. The red and green lines give the predictions by Yoon (2017) and Yoon *et al.* (2010), respectively. Note that Yoon (2017) considers mass-loss enhancement of WR stars during the WC phase, while Yoon *et al.* (2010) adopts a mass-loss prescription that only depends on the helium star luminosity. See Yoon (2017) for more details.

• The photosphere is lifted up from the stellar surface to the wind matter. This makes the effective temperature lowered, the spectral peak shift to a longer wavelength and thus the optical brightness higher, compared to the case without wind. In Figure 7, we show an example with a 9.09 $M_\odot$ helium-deficient SN Ic progenitor model. The surface temperature and radius of this model are $T_* = 1.92 \times 10^5$ K and $R_* = 0.52\ R_\odot$, respectively. The corresponding optical magnitude in the Hubble F555W filter under the black-body assumption is only $M_{\rm F555W} = -0.55$. However, with a mass-loss rate of $\dot{M} = 1.95 \times 10^{-5}\ M_\odot\ {\rm yr}^{-1}$, the effective temperature at the photosphere formed in the extended wind matter is $T_{\rm eff} = 9.97 \times 10^4$ K and the corresponding black-body magnitude is $M_{\rm F555W} = -2.61$. Therefore, this effect alone can make the progenitor appear 7 times brighter in the optical.

• Free-free emission is produced in the wind matter. For the example in Figure 7, the continuum flux in the optical and NIR range is greatly enhanced compared to the black-body spectrum at the effective temperature of the photosphere because of this free-free emission. The corresponding optical magnitude is $M_{\rm F555W} = -3.34$, which is significantly different from the magnitudes obtained with the black body spectra at the effective temperature ($M_{\rm F555W} = -2.61$) and the stellar surface temperature ($M_{\rm F555W} = -0.55$).

• Strong emission lines are formed in the wind, which can significantly affect magnitudes of specific filters. For the example of Figure 7, the optical magnitude from the full spectrum including the emission lines is $M_{\rm F555W} = -4.39$, compared to $M_{\rm F555W} = -3.34$ from the continuum spectrum only.

Therefore, the presence of an optically thick wind from a SN Ib/Ic progenitor can greatly enhance the optical brightness as shown in Figure 8. This would allow us to constrain the mass-loss rate immediately before the SN explosion as discussed in Jung *et al.* (2022). They also find that the color of SN Ib/Ic progenitors would not become systematically bluer for a higher effective temperature, unlike the prediction with the black-body approximation. This implies that the luminosity and effective temperature of a progenitor candidate cannot be properly inferred by comparing the optical data with standard stellar evolution model predictions, unless the wind effects are properly considered.

https://doi.org/10.1017/S1743921322000783 Published online by Cambridge University Press

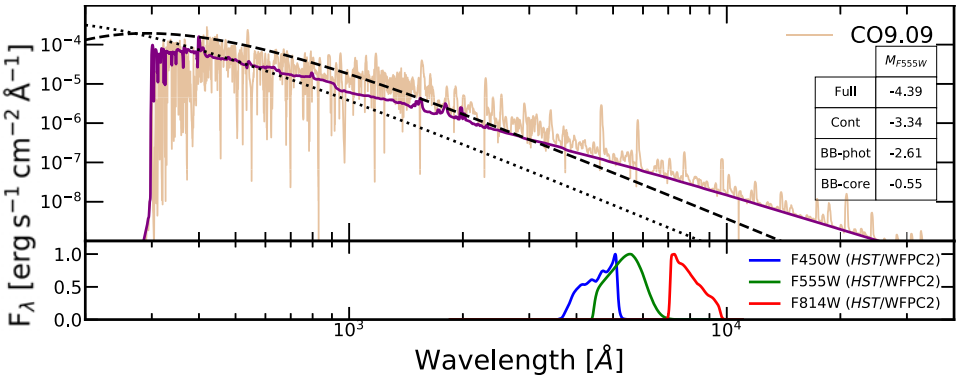

Figure 7. Spectral energy distribution of a helium-deficient SN Ic progenitor model with $M = 9.09\ M_\odot$, $\log L/L_\odot = 5.43$, $T_{\rm surf} = 1.92 \times 10^5$ K, and $R = 0.47 R_\odot$ for a stellar wind mass-loss rate of $1.95 \times 10^{-5}\ M_\odot\ {\rm yr}^{-1}$. The full spectrum was calculated with the non-LTE stellar atmosphere code CMFGEN (Hillier & Miller 1998; Hillier *et al.* 2003). The dotted line gives the black-body spectrum at the surface temperature of the model. The dashed line denotes the black-body spectrum at the effective temperature of the photosphere formed in the wind matter. The purple solid line gives the continuum spectrum. The full spectrum is given by the orange solid line. The figure is taken from Jung *et al.* (2022).

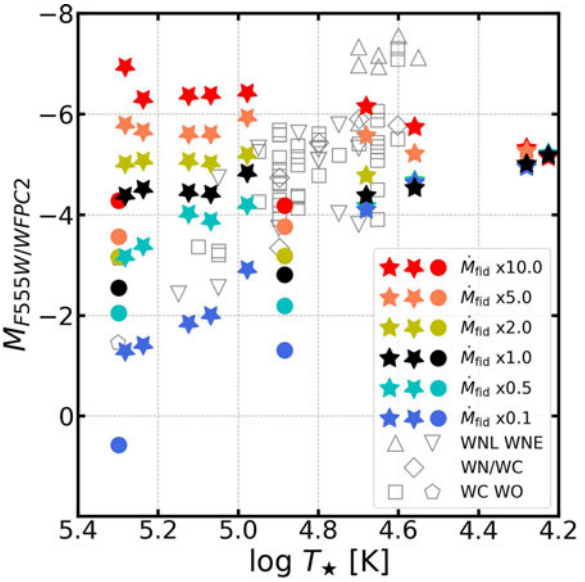

Figure 8. The predicted F555W (HST/WFPC2) filter magnitudes of SNe Ib/Ic progenitors for different mass-loss rates, as a function of the surface stellar temperature. This prediction is made with non-LTE stellar atmosphere models calculated with the CMFGEN code (Hillier & Miller 1998; Hillier *et al.* 2003). The star symbols represent the results from the SN Ib and Ic progenitor models of Yoon (2017) having final masses of 2.91, 2.97, 4.09, 5.05, 5.18, 5.50, 6.16, 7.50, 9.09 $M_\odot$ in the order of decreasing surface temperature. The filled circles denote SN Ic progenitor models of Yoon *et al.* (2019) having final masses of 2.16 and 3.93 $M_\odot$. The black color denotes the result with the fiducial mass-loss rate of helium stars given by Yoon (2017). The results with other mass-loss rates are given by different colors as indicated by the labels in the figure. The open symbols denote Smith v-band filter magnitudes of the Galactic WR star sample of the Potsdam group (Sander *et al.* 2019; Hamann *et al.* 2019). The figure is taken from Jung *et al.* (2022).

https://doi.org/10.1017/S1743921322000783 Published online by Cambridge University Press

5. Implications for iPTF13bvn, SN 2017ein, and SN 2019yvr

So far, there are only three SN Ib/Ic progenitor candidates directly identified in pre-SN optical images: iPTF13bvn (SN Ib; Cao *et al.* 2013; Eldridge & Maund 2016; Folatelli *et al.* 2016), SN 2017ein (SN Ic; Kilpatrick *et al.* 2018; Van Dyk et al. 2018), and SN 2019yvr (SN Ib; Kilpatrick *et al.* 2021). All of these candidates are unusually bright in the optical, compared to our model predictions with the fiducial mass-loss rate given in Figure 8: $M_{\rm F555W} \approx -6.0, -7.5$, and -7.8 for iPTF13bvn, SN 2017ein, and SN 2019yvr, respectively. The optical brightness and color of the iPTF13bvn progenitor candidate might be explained by the lowest mass SN Ib model having an extended helium envelope ($R = 25\ R_\odot$; see also Kim *et al.* 2015) but the other two are too bright to be explained by any fiducial model in Figure 8.

Interestingly, we find that enhanced mass loss shortly before the SN explosion can provide a reasonable solution for the optical properties of these progenitor candidates as discussed in Jung *et al.* (2022). The optical magnitudes and color of the iPTF13bvn progenitor candidate can be achieved in SN Ib progenitor models of $M \simeq 4.0 \cdots 5.0\ M_\odot$ with a mass-loss rate 10 times higher than the fiducial value (i.e., $\dot{M} \approx 5.5 \cdots 8.0 \times 10^{-5} M_\odot\ {\rm yr}^{-1}$; see also Figure 8).

The color of SN 2019yvr progenitor candidate is very red (i.e., $T_{\rm eff} \approx 6800$ K) compared a typical SN Ib progenitor ($T_{\rm eff} = \sim 10^4$ K), but both the color and optical magnitudes of the SN 2019yvr progenitor candidate can be obtained by a SN Ib progenitor model of $\sim 5.0 M_\odot$ with a 50 – 100 times higher mass-loss rate than the fiducial value (i.e., $\dot{M} \approx 4.0 \cdots 8.0 \times 10^{-4} M_\odot\ {\rm yr}^{-1}$) as shown in Figure 9. Note that such a late time mass-loss enhancement from a helium star is indeed predicted in recent stellar models where heating of the envelope via hydrodynamic waves that transports nuclear energy from the core to the outermost layers is considered (Fuller & Ro 2018; Leung *et al.* 2021). Evidence of mass eruption shortly before the SN explosion is also found in some SNe Ib/Ic (e.g., Jin *et al.* 2021). Alternatively, the SN 2019yvr progenitor itself or its comparison might be a yellow supergiant having an extended tenuous hydrogen-rich envelope (Gilkis & Arcavi 2022; Sun *et al.* 2022).

As for the SN 2017ein progenitor candidate, its optical brightness might be roughly explained by a SN Ic progenitor model with ~ 10 times higher than the fiducial value. However, this object seems to be too blue to be explained by our SN Ic progenitor models or by a massive O-type star companion (see Jung et al. 2022 for more details). Future observations need to confirm if this candidate was a real SN progenitor or not by its disappearance.

6. Conluding remarks

SN Ib/Ic progenitors are stripped-envelope stars and thus provide important constraints for stellar evolution models including mass loss via stellar winds and/or binary interactions (Sections 2 and 3). Although WR stars observed in the nearby universe can also provide useful information on SN Ib/Ic progenitors, most of them are still at core helium burning stage and thus their surface properties would become greatly different from now at the pre-SN stage (Yoon *et al.* 2012; Tramper *et al.* 2015). In addition, observed WR stars seem to be too massive (i.e, $M \gtrsim 10 M_\odot$) to explain the observed light curves and spectra of ordinary SNe Ib/Ic.

One of the best ways to understand the exact nature of these progenitors would be direct observation of them before they explode as in the cases of iPTF13bvn, SN 2017ein and SN 2019yvr. However, our recent work indicates that direct comparison of stellar evolution models with the pre-SN observations might be misleading (Jung *et al.* 2022). This is because presence of an optically thick wind can greatly affect optical properties as discussed above. The sensitivity of the optical brightness and color on the wind density

https://doi.org/10.1017/S1743921322000783 Published online by Cambridge University Press

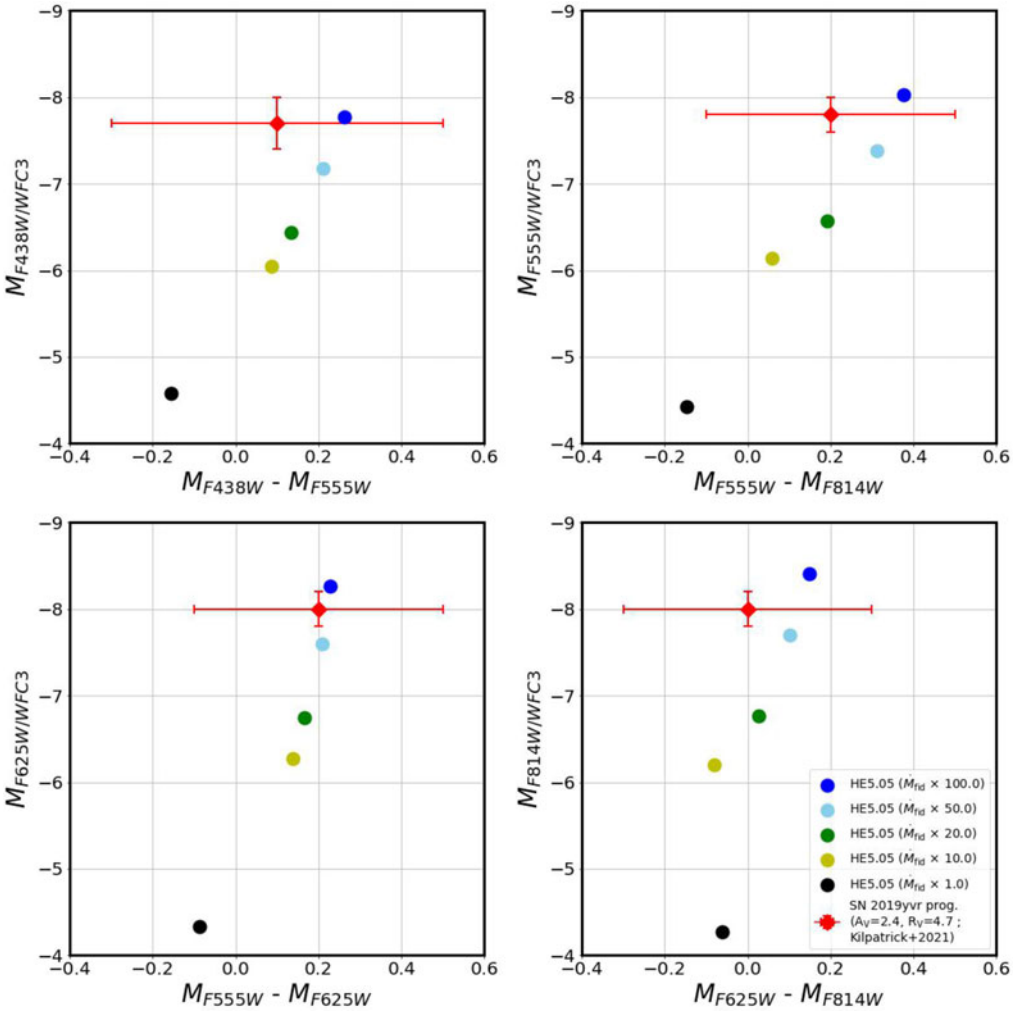

Figure 9. Predicted optical magnitudes and colors for various mass-loss rates (from 1.0 to 100.0 times the fiducial mass-loss rate given by Yoon (2017), as indicated by the labels in the lower right panel) for a 5.05 $M_{\odot}$ helium-rich SN Ib progenitor, compared to the observation of the SN 2019yvr progenitor candidate. This prediction is obtained with the non-LTE stellar atmosphere code CMFGEN. The figure is taken from Jung *et al.* (2022).

(see Section 4), on the other hand, would allow us to make a good constraint on the mass-loss history during the final evolutionary stages of SN Ib/Ic progenitors. Given that signatures of such mass loss can be found in the early-time SN light curves and spectra, combination of progenitor identification and very early-time SN observation in future studies would be important for making good progress towards a better understanding of SN Ib/Ic progenitors.

References

Aguilera-Dena, D.R., Langer, N., Antoniadis, J., et al. 2021 *arXiv:2112.06948*, submitted to A&A

Cano, Z. 2013 *MNRAS*, 434, 1098

Cao, Y., Kasliwal, M.M., Arcavi, I., et al. 2013 *ApJL*, 775, L7

Dessart, L., Hillier, D.J., Li, C., & Woosley, S.E. 2012 *MNRAS*, 424, 2139

Dessart, L., Yoon, S.-C., Aguilera-Dena, D.R., & Langer, N. 2020 *A&A*, 642, 106

https://doi.org/10.1017/S1743921322000783 Published online by Cambridge University Press

Drout, M.R., Soderberg, A.M., Gal-Yam, A., et al. 2011 *ApJ*, 741, 97
Eldridge, J.J., Fraser, M., & Smartt, S., et al. 2013 *MNRAS*, 436, 774
Eldridge, J.J., & Maund, J.R. 2016 *MNRAS*, 461, L117
Farrell, E.J., Groh, J.H., Meynet, G., Eldridge, J.J. 2020 *MNRAS*, 494, 53
Folatelli, G., Van Dyk, S.D., Kuncarayakti, H., et al. 2016 *ApJL*, 825, L22
Fremling, C., Sollerman, J., Kasliwal, M.M., et al. 2018 *A&A*, 618, 37
Fuller, J., & Ro, S. 2017 *MNRAS*, 476, 1853
Gilkis, A., & Arcavi I. 2022 *MNRAS*, 511, 691
Gilkis, A., Vink, J., Eldridge, J.J., & Tout, C. 2019 *MNRAS*, 486, 4451
Hachinger, S., Mazzali, P.A., Taubenberger, S., et al. 2012 *MNRAS*, 422, 70
Hainich, R., Ruehiling, U., Todt, H., et al. 2014 *A&A*, 565, 27
Hamann, W.-R., Graefener, G., & Liermann, A. 2006 *A&A*, 457, 1015
Hamann, W.R., Graefener, G., Liermann, A., et al. 2019 *A&A*, 625, A57
Hillier, D.J., Lanz, T., Heap, S.R., et al. 2003 *ApJ*, 588, 1039
Hillier, D.J., & Miller, D.L. 1998 *ApJ*, 496, 407
Jin, H., Yoon, S.-C., & Blinnikov, S. 2021 *ApJ*, 910, 68
Jung, M.-K. Yoon, S.-C., & Kim, H.-J. 2022 *ApJ*, 925, 216
Kilpatrick, C.D., Drout, M.R., Auchettl, K., et al. 2021 *MNRAS*, 504, 2073
Kim, H.-J., Yoon, S.-C., & Koo, B.-C. 2015 *ApJ*, 809, 131
Kilpatrick, C.D., Takaro, T., Foley, R.J., et al. 2018 *MNRAS*, 480, 2072
Langer, N. 2012 *ARA&A*, 50, 107
Leung, S.-C., Wu., S., & Fuller, J. 2021 *ApJ*, 923, 41
Liu, Y.-Q., Modjaz, M., Biaco, F., & Graur, O. 2016 *ApJ*, 827, 90
Lyman, J.D., Bersier, D., James, P.A. 2016 *MNRAS*, 457, 328
Lucy, L.B. 1991 *ApJ*, 383, 308
Menon, A., & Heger, A. 2016 *MNRAS*, 469, 46
Morris, Th., & Podsiadlowski 2007 *Science*, 315, 1103
Podsiadlowski, Ph., Joss, P.C., & Rappaport, Sl. 1990 *A&A*, 227, L9
Prentice, S.J., Ashall, C., James, P.A., et al. 2019 *MNRAS*, 485, 1559
Sander, A., Hamann, W.R., & Todt, H. 2012 *A&A*, 540, 144
Sander, A., Hamann, W.R., Todt, H., et al. 2019 *A&A*, 621, A92
Sander, A., Vink, J.S., Hamann, W.-R. 2020 *MNRAS*, 491, 440
Shahbandeh, M., Hsiao, E.Y., & Ashall, C. et al. 2021, *ApJ*, 925, 175
Shenar, T., Gilkis, A., Vink, J.S., Sana, H., & Sander, A.A.C. 2020 *A&A*, 634, 79
Sun, N.-C., Maund, J.R., Crowther, P.A., et al. 2022 *MNRAS*, 510, 3701
Teffs, J., Ertl, T., Mazzali, P., et al. 2020 *MNRAS*, 499, 730
Tramper, F., Straal, S., & Sanyal, D., et al. 2015, *A&A*, 581, A110
Smartt, S. 2015, *PASA*, 32, e016
Smith, N. 2014, *ARA&A*, 52, 487
Swartz, D. A. 1991 *ApJ*, 373, 604
Taddia, F., Sollerman, J., Ledoudas, G., et al. 2018, *A&A*, 609, A136
Urushibata, T., Takahashi, K., Umeda, H., Yoshida, T. 2018, *A&A*, 609, A136
Williamson, M., Kerzendorf, W., & Modjaz, M. 2021 *ApJ*, 908, 150
Van Dyk, S. D., Zheng, W, Brink, T. G., Filippenko, A. V. , Milisavljevic, D, Andrews, J. E., Smith, N., Cignoni, M, Fox, O. D., Kelly, P. L., Adamo, A., Yunus, S., Zhang, K., Kumar, S., 2018, *ApJ*, 860, 2
Vink, J.S. 2017, *A&A*, 607, 8
Vink, J.S. 2022, *ARA&A*, in press
Woosley, S.E. 2019 *ApJ*, 878, 49
Yoon, S.-C. 2015, *PASA*, 32, e015
Yoon, S.-C. 2017, *MNRAS*, 470, 3970
Yoon, S.-C., Chun, W., Tostov, A., Blinnikov, S., & Dessart, L. 2019, *ApJ*, 872, 174
Yoon, S.-C., Dessart, L., & Clocchiatti, A. 2017, *ApJ*, 840, 10
Yoon, S.-C., Graefener, G., Vink, J.S., Kozyreva, A., & Izzard, R.G. 2012, *A&A*, 544, L11
Yoon, S.-C., Woosley, S.E., & Langer, N. 2010 *ApJ*, 725, 940